

Proton-Coupled Intervalence Charge Transfer: Concerted Processes

Ramachandran Balasubramanian,[†] Geneviève Blondin,[‡] Juan Carlos Canales,[†] Cyrille Costentin,[†] Jean-Marc Latour,[‡] Marc Robert,[†] and Jean-Michel Savéant^{*,†}

[†]Université Paris Diderot, Sorbonne Paris Cité, Laboratoire d'Electrochimie Moléculaire, Unité Mixte de Recherche Université - CNRS 7591, Bâtiment Lavoisier, 15 rue Jean de Baïf, 75205 Paris Cedex 13, France

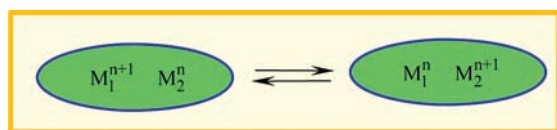
[‡]UJF-Grenoble 1/CEA-DSV-iRTSV/CNRS, Laboratoire de Chimie et Biologie des Métaux-pmb, UMR 5249, Grenoble F-38054, France

Supporting Information

ABSTRACT: The kinetics of proton-induced intervalence charge transfer (IVCT) may be measured electrochemically by generating one of the members of the IVCT couple in situ and following its conversion by means of the electrochemical signature of the other member of the couple. In the case of the diiron complex taken as an example, the reaction kinetics analysis, including the H/D isotope effect, clearly points to the prevalence of the concerted proton–intervalence charge transfer pathway over the stepwise pathways. A route is thus open toward systematic kinetic studies of proton-induced IVCT aiming at uncovering the main reactivity parameters and the factors that control the occurrence of concerted versus stepwise pathways.

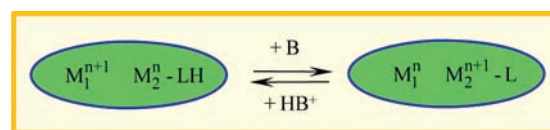
For almost four decades,¹ intervalence charge transfer (IVCT) has attracted continuously renewed experimental and theoretical attention,² being illustrated by organic systems³ and mostly by transition-metal complex systems.^{4–8} In the latter case, these systems involve two metal centers that may be identical or not, although systems comprising more than two metal centers have also been considered. The metal centers are held together by a common ligand and may or may not be connected by a more or less conducting ligand. The various situations are symbolized by the general diagram shown in Scheme 1.

Scheme 1



Electron transfer can be triggered by proton transfer. Examples of such electron transfer have been reported for dinuclear complexes upon deprotonation of a bridging ligand.^{9–11} In addition, such symmetric dinuclear mixed-valent systems may present localized or delocalized valences depending on pH. A single example of IVCT triggered by a proton transfer on a terminal ligand (Scheme 2) has been reported to date.¹² B is an external base that serves as an acceptor for the proton delivered by the protonated ligand LH, thus triggering the IVCT, in which an electron is transferred from the right-

Scheme 2



hand to the left-hand metal center. The reaction in Scheme 2 is thus a typical proton-coupled electron transfer (PCET) process. The system is a bistable construct wherein the passage from one state to the other may be triggered by a change in pH.

PCET reactions are currently under active scrutiny from both experimental and theoretical viewpoints.¹³ Mechanism analysis based on the kinetics of the reaction has mostly focused on the distinction between stepwise pathways in which protonation and electron transfer take place successively [initial proton transfer followed by electron transfer (PET pathway) or vice versa (EPT pathway)] and a concerted proton–electron transfer (CPET) pathway in which the two events take place in concert. The advantage of the CPET pathway over the stepwise pathways is that it avoids going through high-energy intermediates. This is a way of exploiting the driving force advantage offered by the coupling between proton and electron transfers, an advantage that becomes effective if the kinetic price that may have to be paid is not too high. A delineation of the various pathways in the present case of proton-coupled IVCT is summarized in Scheme 3. Such a mechanism analysis requires the determination of the rate constant of the PCET reaction, which has not been the case for the systems in which proton transfer triggers IVCT as reported to date.

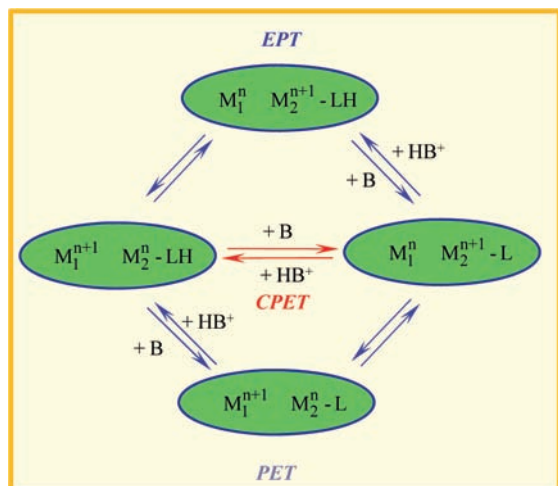
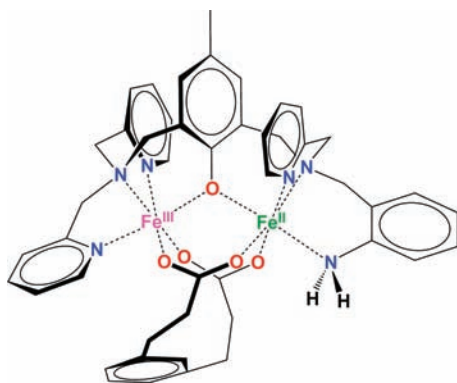
The purpose of the present communication is to describe a method that allows such rate constant determinations to aid in establishing the reaction mechanism. The main thrust in this connection is the distinction between the concerted and stepwise pathways. The method is based on the recording and analysis of the cyclic voltammetric responses of the complexes involved. It is illustrated by the diiron complex depicted in Scheme 4, where, with reference to Schemes 2 and 3, $M_1 = M_2 = \text{Fe}$, $n = \text{II}$, and the ligand L is defined in Scheme 4.¹⁴

The first step of the analysis deals with the description of the thermodynamic framework in the form of a Pourbaix diagram (variation of the apparent standard potentials of the system, E^0 ,

Received: August 10, 2011

Published: January 18, 2012

Scheme 3

Scheme 4. $\text{Fe}^{\text{III}}\text{Fe}^{\text{II}}\text{LH}^a$ 

^aOnly the H atoms at the site where proton transfer occurs are shown.

with pH) as reported in Figure 1, which shows the diagram itself and the various experiments that allowed its establishment. The four cyclic voltammograms (CVs) allowed the derivation of the four characteristic standard potentials; the most negative one is approximate since the corresponding wave is not reversible. The pK of $\text{Fe}^{\text{III}}\text{Fe}^{\text{II}}\text{LH}$ was obtained from the variation of its UV-vis spectrum upon addition of NEt_3 (Figure 1f,g) according to the expression

$$\frac{A - A_{n=0}}{A_{n \rightarrow \infty} - A_{n=0}} = \frac{n + 1 - \sqrt{(n + 1)^2 - 4n(1 - K)}}{2(1 - K)}$$

in which n is the number of NEt_3 equivalents and K is related to the pK of interest as

$$K = 10^{pK_{\text{Fe}^{\text{III}}\text{Fe}^{\text{II}}\text{LH}} - pK_{\text{Et}_3\text{NH}^+}}$$

K was thus found to be 0.1, which, in combination with $pK_{\text{Et}_3\text{NH}^+} = 18.6$,¹⁵ gave $pK_{\text{Fe}^{\text{III}}\text{Fe}^{\text{II}}\text{LH}} = 17.6$. These E^0 and pK data allowed the Pourbaix diagram shown in Figure 1 to be drawn, thus leading to $pK_{\text{Fe}^{\text{III}}\text{Fe}^{\text{II}}\text{LH}} = 9.9$ and $pK_{\text{Fe}^{\text{II}}\text{Fe}^{\text{III}}\text{LH}} \approx 27.9$ [see the Supporting Information (SI) for details].

Once the thermodynamic scene had been set, we employed the following electrochemical method to determine the rate constants of the proton-coupled IVCT on the basis of the reactions depicted in the scheme shown in Figure 2a. Starting with the initial complex $\text{Fe}^{\text{III}}\text{Fe}^{\text{III}}\text{LH}$ in the presence of a mixture of B (i.e., NEt_3) and its corresponding acid BH^+ , the potential

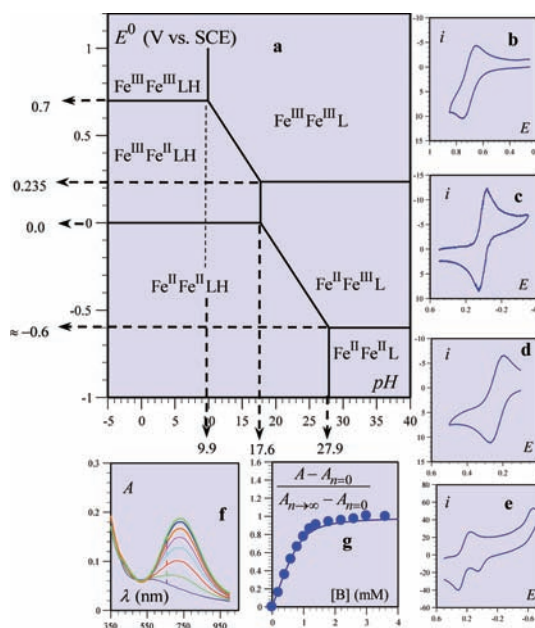


Figure 1. (a) Pourbaix diagram. (b–e) CVs of 0.65 mM $\text{Fe}^{\text{III}}\text{Fe}^{\text{II}}\text{LH}$ complex in $\text{CH}_3\text{CN} + 0.1 \text{ M NBu}_4\text{BF}_4$ on a 3 mm diameter glassy carbon disk electrode at scan rates (ν) of (b–d) 0.1 and (e) 0.5 V/s; (b) oxidation; (c) reduction; (d) oxidation in the presence of 10 equiv of NEt_3 ; (e) reduction in the presence of 10 equiv of NEt_3 . (f) Increase in the UV-vis band of the $\text{Fe}^{\text{III}}\text{Fe}^{\text{II}}\text{L}$ complex upon addition of NEt_3 to $\text{Fe}^{\text{III}}\text{Fe}^{\text{II}}\text{LH}$. (g) Variation of the normalized peak absorbance with the number of NEt_3 equivalents, n .

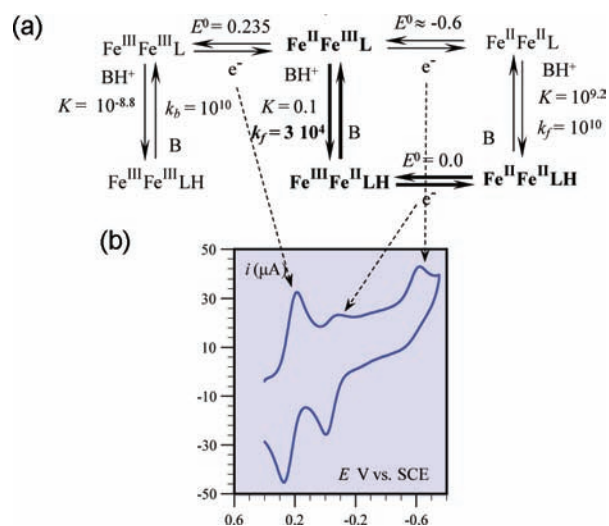


Figure 2. (a) Reaction scheme for determining the rate constants of proton-coupled IVCT. Standard potentials (E^0) are given in V vs SCE and forward (k_f) and backward (k_b) rate constants in $\text{M}^{-1} \text{ s}^{-1}$. K 's are equilibrium constants. (b) CV of 0.65 mM $\text{Fe}^{\text{III}}\text{Fe}^{\text{II}}\text{LH}$ complex in $\text{CH}_3\text{CN} + 0.1 \text{ M NBu}_4\text{BF}_4$ on a 3 mm diameter glassy carbon disk electrode at $\nu = 1 \text{ V/s}$ in the presence of a mixture of NEt_3 (4 mM) and Et_3NH^+ (2 mM) after a pre-electrolysis at 0.4 V to convert the initial complex into $\text{Fe}^{\text{III}}\text{Fe}^{\text{III}}\text{L}$.

of the working electrode was set at 0.4 V vs SCE for an in situ pre-electrolysis (10 s), at the end of which $\text{Fe}^{\text{III}}\text{Fe}^{\text{III}}\text{L}$ was the only complex present in the solution surrounding the electrode, together with a preset mixture of B and BH^+ . At the first cathodic peak (Figure 2b), $\text{Fe}^{\text{III}}\text{Fe}^{\text{III}}\text{L}$ was reduced at ca. 0.235 V to give $\text{Fe}^{\text{II}}\text{Fe}^{\text{III}}\text{L}$, which, thanks to the BH^+ present, was

partly converted into $\text{Fe}^{\text{III}}\text{Fe}^{\text{II}}\text{LH}$ according to the reaction of interest. Addition of BH^+ in these experiments was necessary to ensure that its concentration was constant throughout the diffusion–convection layer. $\text{Fe}^{\text{III}}\text{Fe}^{\text{II}}\text{LH}$ was reduced at ca. 0.0 V, whereas the remainder of $\text{Fe}^{\text{II}}\text{Fe}^{\text{III}}\text{L}$ was reduced at a much more negative potential (ca. -0.6 V). The second wave on the voltammogram involved a typical chemical reaction preceding electron transfer (CE) process¹⁶ (bold arrows and symbols in Figure 2a) in which the electroactive species, $\text{Fe}^{\text{III}}\text{Fe}^{\text{II}}\text{LH}$, was reduced at the electrode and continuously regenerated by the transformation of $\text{Fe}^{\text{II}}\text{Fe}^{\text{III}}\text{L}$ with an efficiency that depended on the scan rate (ν). The second wave decreased with increasing NEt_3 concentration at a given ν (Figure 3a) and with increasing

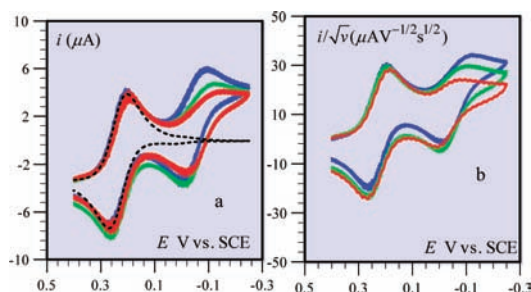


Figure 3. CVs of 0.65 mM $\text{Fe}^{\text{III}}\text{Fe}^{\text{II}}\text{LH}$ complex after a 10 s pre-electrolysis at 0.4 V in the presence of 2 mM Et_3NH^+ . (a) Variation with the NEt_3 concentration at $\nu = 0.05$ V/s: 4 mM (blue); 8 mM (green); 12 mM (red). Dotted line: simulation of the first wave. (b) Variation with ν at $[\text{NEt}_3] = 8$ mM: 0.05 V/s (blue); 0.2 V/s (green); 1 V/s (red). The current at the starting potential was set to zero for the sake of an easier comparison.

ν at a given NEt_3 concentration (Figure 3b), as expected for a CE mechanism.¹⁶ The third wave was consistently observed to vary in the opposite manner.

With knowledge of the equilibrium constant of the reaction (see the above thermodynamic analysis), the second wave of the voltammograms could be simulated^{17,18} according to the CE mechanism (bold arrows and symbols in Figure 2a) and compared to the experimental data after subtraction of the current due to the first wave, corresponding to $\text{Fe}^{\text{II}}\text{Fe}^{\text{III}}\text{L}$ reduction (its simulation is represented as a dashed line in Figure 3a). The rate constant of the PCET reaction for conversion of $\text{Fe}^{\text{II}}\text{Fe}^{\text{III}}\text{L}$ into $\text{Fe}^{\text{III}}\text{Fe}^{\text{II}}\text{LH}$ was found to be $\log(k_f) = 4.5 \pm 0.1$. Examples of simulations are given in Figure 4 (other simulations and details are available in the SI).

The results gathered to this point are compatible with the CPET pathway but also with the two stepwise pathways, PET and EPT, as shown in Schemes 3 and 5. To discriminate between these mechanisms, the same experiments were repeated with another base, pyrrolidine ($\text{p}K = 19.6$)^{15b} (see the SI), which gave $\log(k_f) = 4.0 \pm 0.1$. Relating the decrease in the rate constant to the 1 pK unit decrease of the driving force entails a value of the symmetry factor $\alpha = (d \log k_f / d \log K) \approx 0.5 \pm 0.05$.¹⁹ This value is compatible with the CPET mechanism insofar it is characterized by a quadratic activation driving force law,²⁰ which can be linearized over the small range of driving forces considered here. Such a value of the symmetry factor is not compatible with either of the two stepwise pathways for the following reasons. With simple amines such as those used here, the rate constants of the protonation and deprotonation reactions are expected to be at the diffusion limit in the thermodynamically favorable direction,²¹ as sketched in

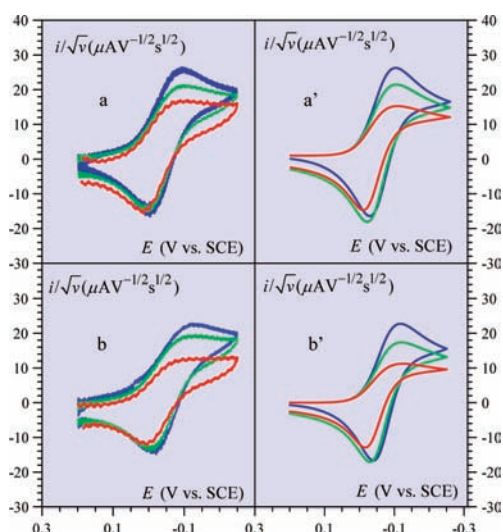
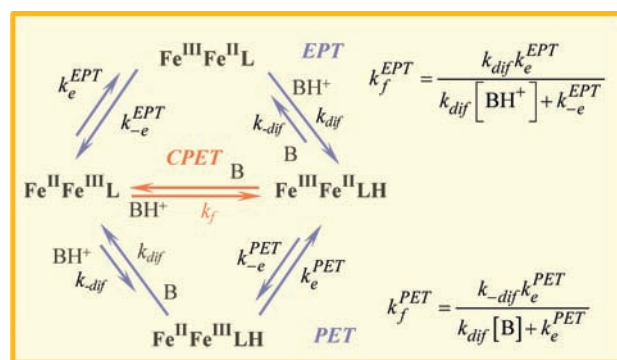


Figure 4. CVs of 0.65 mM $\text{Fe}^{\text{III}}\text{Fe}^{\text{II}}\text{LH}$ complex under the same conditions as in Figure 3 after subtraction of the simulated first wave. ν (V/s): 0.05 (blue) 0.2 (green) 1 (red). $[\text{Et}_3\text{NH}^+] = 2$ mM. (a, a') $[\text{NEt}_3] = 4$ mM; (b, b') $[\text{NEt}_3] = 8$ mM. (a, b) experimental; (a', b') simulated (see the text).

Scheme 5



Scheme 5. The resulting expressions for k_f for the two stepwise mechanisms are given in Scheme 5. It is seen that α is predicted to be 1 for the PET pathway and 0 for the EPT pathway, thus ruling out these two possibilities.^{19b}

If the reaction does follow the CPET pathway, an H/D kinetic isotope effect (KIE) would be expected. That this is indeed the case is shown in Figure 5, where experiments with NEt_3 as a base performed in the presence of 1% MeOH were repeated in the presence of 1% MeOD. It is a purely kinetic effect because the equilibrium constant K had the same value in the presence of either 1% MeOH or 1% MeOD, as checked by UV–vis experiments (see the SI). A quantitative estimation of the effect ($\text{KIE} = 2 \pm 0.2$)²² was obtained by means of simulations (see the SI). A clear confirmation that the proton-coupled IVCT reaction follows the concerted pathway is thus provided.^{22b} No significant KIE would be expected with the stepwise pathways since, as already noted, the rate constants of the protonation and deprotonation reactions would be at the diffusion limit in the thermodynamically favorable direction.

In summary, we have shown that the kinetics of proton-induced IVCT may be measured electrochemically by generating one of the members of the IVCT couple in situ and following its conversion by means of the electrochemical signature of the other member of the couple.

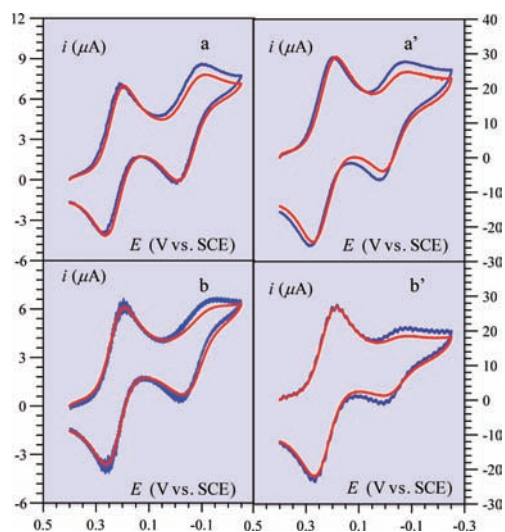


Figure 5. CVs of 0.65 mM $\text{Fe}^{\text{III}}\text{Fe}^{\text{II}}\text{LH}$ complex under the same conditions as in Figure 3 in the presence of 1% MeOH (blue) or 1% MeOD (red). $[\text{Et}_3\text{NH}^+] = 2$ mM. (a, a') $[\text{NEt}_3] = 4$ mM; (b, b') $[\text{NEt}_3] = 12$ mM. (a, b) $\nu = 0.05$ V/s; (a', b') $\nu = 1$ V/s.

In the case of the diiron complex used as an example in the present study, application of the method to the determination of the H/D isotope effect and variation of the rate constant with the driving force clearly points to the prevalence of the concerted proton–intervalence charge transfer pathway over the stepwise pathways.

A route is thus open toward a systematic kinetic study of proton-induced IVCT aimed at uncovering the main reactivity parameters and the factors that control the occurrence of concerted versus stepwise pathways. Work is in progress to investigate the dependence of the CPET intervalence kinetics upon temperature in order to evaluate reorganization and proton tunneling factors.

■ ASSOCIATED CONTENT

📄 Supporting Information

Experimental details and additional simulations. This material is available free of charge via the Internet at <http://pubs.acs.org>.

■ AUTHOR INFORMATION

Corresponding Author

saveant@univ-paris-diderot.fr

■ ACKNOWLEDGMENTS

Partial financial support from the Agence Nationale de la Recherche (ANR 2010 BLAN 703) is gratefully acknowledged.

■ REFERENCES

- (1) Creutz, C.; Taube, H. *J. Am. Chem. Soc.* **1973**, *95*, 1086.
- (2) Reimers, J. R.; Wallace, B. B. *Philos. Trans. R. Soc. London, Ser. A* **2008**, *366*, 15.
- (3) Nelsen, S. F. *Adv. Phys. Org. Chem.* **2006**, *41*, 183.
- (4) Ceccon, A.; Santi, S.; Orian, L.; Bisello, A. *Coord. Chem. Rev.* **2004**, *248*, 683.
- (5) Evangelio, E.; Ruiz-Molina, D. *Eur. J. Inorg. Chem.* **2005**, 2957.
- (6) (a) D'Alessandro, D. M.; Keene, F. R. *Chem. Rev.* **2006**, *106*, 2270. (b) D'Alessandro, D. M.; Keene, F. R. *Chem. Soc. Rev.* **2006**, *35*, 424.
- (7) Kaim, W.; Sarkar, B. *Coord. Chem. Rev.* **2007**, *251*, 584.
- (8) Aguirre-Etcheverry, P.; O'Hare, D. *Chem. Rev.* **2010**, *110*, 4839.

- (9) (a) Haga, M. A.; Ano, T.; Kano, K.; Yamabe, S. *Inorg. Chem.* **1991**, *30*, 3843. (b) Haga, M. A.; Ali, M. M.; Koseki, S.; Fujimoto, K.; Yoshimura, A.; Nozaki, K.; Ohno, T.; Nakajima, K.; Stufkens, D. J. *Inorg. Chem.* **1996**, *35*, 3335.

- (10) Rocha, R. C.; Toma, H. E. *Inorg. Chem. Commun.* **2001**, *4*, 230.

- (11) Baitalik, S.; Dutta, S.; Biswas, P.; Florke, U.; Bothe, E.; Nag, K. *Eur. J. Inorg. Chem.* **2010**, 570.

- (12) Neyhart, G. A.; Meyer, T. J. *Inorg. Chem.* **1986**, *25*, 4807.

- (13) *Chemical Reviews* special issue on PCET: *Chem. Rev.* **2010**, *110*, issue 12.

- (14) The synthesis and characteristics of the complex (including an X-ray crystal structure) as well as the demonstration that it undergoes IVCT upon deprotonation are the subject of a separate publication: Gouré, E.; Thiabaud, G.; Carboni, M.; Gon, N.; Dubourdeaux, P.; Garcia-Serres, R.; Clémancey, M.; Oddou, J.-L.; Robin, A. Y.; Jacquamet, L.; Dubois, L.; Blondin, G.; Latour, J.-M. *Inorg. Chem.* **2011**, *50*, 6408.

- (15) (a) Two values of $\text{p}K_{\text{Et}_3\text{NH}^+}$ are given in ref 15b: 18.7 and 18.5. We therefore used the value 18.6 ± 0.1 , giving $\text{p}K_{\text{Fe}^{\text{III}}\text{Fe}^{\text{II}}\text{LH}} = 17.6 \pm 0.1$.

- (b) Izutsu, K. *Acid–Base Dissociation Constants in Dipolar Aprotic Solvents*; Blackwell: Boston, 1990; pp 17–35.

- (16) Savéant, J.-M. *Elements of Molecular and Biomolecular Electrochemistry: An Electrochemical Approach to Electron Transfer Chemistry*; Wiley: Hoboken, NJ, 2006; Chapter 2.

- (17) Using the DigiElch software: Rudolph, M. *J. Electroanal. Chem.* **2003**, *543*, 23.

- (18) The protonation reactions in the fully oxidized and fully reduced states are thermodynamically very unfavorable and very favorable, respectively. Their rate constants were consequently considered to be at the diffusion limit in the favorable direction. The standard rate constant for the first electrode reaction ($\text{Fe}^{\text{III}}\text{Fe}^{\text{III}}\text{L}/\text{Fe}^{\text{II}}\text{Fe}^{\text{III}}\text{L}$) was taken as equal to 0.1 cm/s to take into account the slight electrochemical irreversibility of the corresponding wave; the value for the second electrode reaction ($\text{Fe}^{\text{III}}\text{Fe}^{\text{II}}\text{LH}/\text{Fe}^{\text{II}}\text{Fe}^{\text{II}}\text{LH}$) was taken at 1 cm/s. The solution electron transfer reaction, $\text{Fe}^{\text{III}}\text{Fe}^{\text{II}}\text{LH} + \text{Fe}^{\text{II}}\text{Fe}^{\text{III}}\text{L} \rightleftharpoons \text{Fe}^{\text{III}}\text{Fe}^{\text{III}}\text{L} + \text{Fe}^{\text{II}}\text{Fe}^{\text{II}}\text{LH}$, has little effect; its rate constant was considered to be at the diffusion limit in the favorable direction. The diffusion coefficients were taken as equal to 10^{-5} for all of complexes and 5×10^{-5} $\text{cm}^2 \text{s}^{-1}$ for NEt_3 and Et_3NH^+ . Finite diffusion with a convection layer of 0.01 cm was employed to take into account natural convection in order to get a correct description of the pre-electrolysis procedure.

- (19) (a) A larger variation of the driving force could not be achieved because the use of a stronger base led to a CE current that was too small to be measured reliably. (b) In spite of the modest variation of the driving force that could be achieved, the value of α is clearly not compatible with the stepwise pathways.

- (20) (a) The quadratic models developed for homogeneous^{20b} and electrochemical^{20c} CPET reactions may be extended to the present intervalence CPET reaction. (b) Hammes-Schiffer, S.; Stuchebrukhov, A. I. *Chem. Rev.* **2010**, *110*, 6939. (c) Costentin, C.; Robert, M.; Savéant, J.-M. *Acc. Chem. Res.* **2010**, *43*, 1019.

- (21) *Proton Transfer Reactions*; Caldin, E., Gold, V., Eds.; Wiley: New York, 1975.

- (22) (a) Although the accuracy of the determination of k_f was 20%, performing the 1% MeOH and 1% MeOD experiments consecutively resulted in better precision, leading to an absolute error of ± 0.2 in the H/D KIE. (b) A value of 2 is commonly found for the H/D KIE in electrochemical CPET reactions.^{20c}